frontiers | Frontiers in Communications and Networks

ORIGINAL RESEARCH
published: 30 May 2022
doi: 10.3389/frcmn.2022.859809

EMF-Aware Probabilistic Shaping Design for Hardware-Distorted Communication Systems

Sidrah Javed[1], Ahmed Elzanaty[2], Osama Amin[1], Mohamed-Slim Alouini[1] and Basem Shihada[1]*

[1]CEMSE Division, King Abdullah University of Science and Technology (KAUST), Thuwal, Saudi Arabia, [2]Institute for Communication Systems (ICS), University of Surrey, Guildford, United Kingdom

The fifth-generation cellular network requires dense installation of radio base stations (BS) to support the ever-increasing demands of high throughput and coverage. The ongoing deployment has triggered some health concerns among the community. To address this uncertainty, we propose an EMF-aware probabilistic shaping design for hardware-distorted communication systems. The proposed scheme aims to minimize human exposure to radio frequency (RF) radiations while achieving the target throughput using probabilistic shaping. The joint optimization of the transmit power and nonuniform symbol probabilities is a non–convex optimization problem. Therefore, we employ alternate optimization and successive convex approximation to solve the subsequent problems. Our findings reveal a significant reduction in the users' exposure to EMF while achieving the requisite quality of service with the help of probabilistic shaping in a hardware-distorted communication system.

Keywords: asymmetric signaling, error probability analysis, hardware impairments, improper noise, non-uniform probabilities, radiation exposure

OPEN ACCESS

Edited by:
Mohamed Saad, University of Sharjah, United Arab Emirates

Reviewed by:
Gabriella Tognola, National Research Council (CNR—EIIT), Italy
Saeed Abdallah, University of Sharjah, United Arab Emirates

****Correspondence:***
Sidrah Javed
sidrah.javed@kaust.edu.sa

Specialty section:
This article was submitted to Communications Theory, a section of the journal Frontiers in Communications and Networks

Received: *21 January 2022*
Accepted: *04 April 2022*
Published: *30 May 2022*

Citation:
Javed S, Elzanaty A, Amin O, Alouini M-S and Shihada B (2022) EMF-Aware Probabilistic Shaping Design for Hardware-Distorted Communication Systems. Front. Comms. Net 3:859809. doi: 10.3389/frcmn.2022.859809

1 INTRODUCTION

The next-generation wireless communication networks are expected to fulfill the ever-increasing demands of higher data rates, ultra-reliability, minimal latency, high energy efficiency, and massive connectivity for many users/devices (Latva-aho et al., 2020). The fifth-generation (5G) wireless technology is envisioned to support numerous diverse services, such as enhanced mobile broadband (eMBB), ultra-reliable low latency communication (URLLC), and massive machine-type communication (mMTC) (Wan et al., 2018). Some of the new spectra allocated for 5G deployments, for example, millimeter waves, suffer from relatively high path loss, limiting the coverage area. Thus, network densification becomes essential for achieving the promised data rate, which can be realized over space [e.g., dense deployment of base stations (BSs) in small cells] and frequency (large segments of the RF spectrum in diverse bands) (Bhushan et al., 2014).

Installation of 5G cellular technology with extreme node and network densification (with BSs being closer to users) is raising health concerns about the impact of electric and magnetic fields (EMFs) exposure on the population. These worries have sparked several protests against 5G technology and led to some attacks on the 5G BSs (Elzanaty et al., 2021). Recently, anti-5G protests have been held in 30 countries around the world against the threat of 5G wireless technology to public health, the environment, and privacy.

Indeed, the thermal effect is the only proven health impact from RF nonionizing short-term exposure. Therefore, it is necessary to keep the radiation intensity below specific values defined by the

exposure regulations and guidelines, such as those of the Federal Communications Commission (FCC) and the International Commission on Non-Ionizing Radiation Protection (ICNIRP) (Buchner and Rivasi, 2020). Nevertheless, there is a debate about severe health impacts due to long-term exposure to EMF (National Toxicology Program, 2018a,b; Vornoli et al., 2019). Hence, the International Agency for Research on Cancer (IARC) classified RF radiation as "possibly carcinogenic to humans" (Vornoli et al., 2019; Group, 2013; Wilbourn et al., 1986).

Recently, a comprehensive study revealed that exposure due to the uplink (UL) from user equipment (UE) is higher than from the BS due to the proximity of the UE to the user (Lou et al., 2021). Another work has proposed an architectural solution to minimize the EMF exposure using reconfigurable intelligent surfaces (Ibraiwish et al., 2022). Another study focused on meticulous cellular network planning to limit exposure from the BSs exploiting MIMO while ensuring coverage and capacity constraints (Matalatala et al., 2018). From the regulatory aspects, some possible risk mitigation strategies are dismission of legacy 2G/3G/4G technologies and reduction of emissions from noncellular sources (Chiaraviglio et al., 2021).

Nevertheless, as mentioned earlier, the EMF exposure–based research does not consider any hardware impairments, which can drastically affect the system performance, such as raising the noise floor. For instance, in order to reach the target data rates in eMBB, hardware distortion (HWD) should be mitigated. Generally, users send a much higher power, escalating their RF exposure to achieve the target rate. The users may still not reach the required throughput due to the saturation for the data rate at a higher SNR as the distortion noise increases with the transmit power.

HWD requires some meticulously designed systems to compensate for its effect and mitigate performance loss. Improper Gaussian signaling (IGS) is an effective compensation signaling scheme that can alleviate the impact of several interference and imperfection sources (Javed et al., 2019). However, realizing the IGS comes with inherent problems of the unbounded peak-to-average power ratio and high detection complexity (Santamaria et al., 2018; Javed et al., 2020). As a consequence, researchers employ finite discrete asymmetric signaling (AS) schemes that can be achieved by geometric shaping (GS), probabilistic shaping (PS), or hybrid shaping (HS) (Elzanaty and Alouini, 2022; Javed et al., 2021). In this work, we propose asymmetric signaling by adopting PS to tackle improper HWD and minimize EMF exposure to the users while maintaining throughput quality of service (QoS). The contributions of this study are summarized as follows:

- We model HWD and EMF exposure in the next-generation wireless cellular network. We present an appropriate receiver and rigorous error probability analysis considering the improper distortion noise.
- We propose probability shaping as a form of asymmetric signaling to effectively mitigate improper HWDs and reduce EMF exposure while maintaining QoS in terms of user throughput.

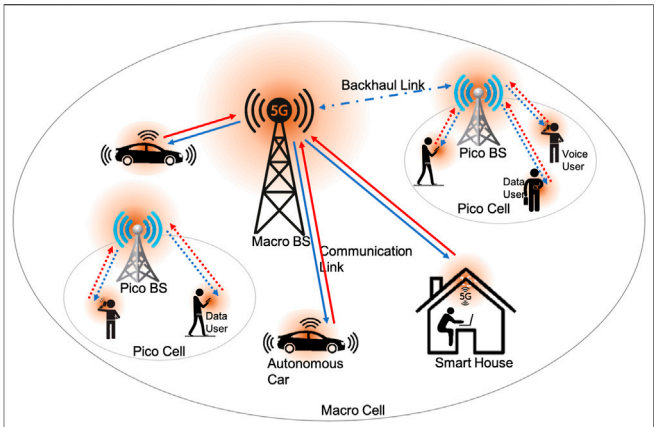

FIGURE 1 | EMF exposure from 5G network infrastructure.

- We employ alternate optimization to jointly design the transmit power of users and nonuniform symbol probabilities. We further use successive convex approximation and the Newton–Raphson method to solve subsequent problems.

The rest of the article is organized such that **Section 2** illustrates the system description and adopted models to characterize the radiation exposure and HWD. The error probability analysis is carried out in **Section 3**, while **Section 4** covers the problem formulation and optimization framework. Numerical results are presented in **Section 5**, followed by the conclusion in **Section 6**.

2 SYSTEM DESCRIPTION

In this section, we quantify the EMF exposure of the human population in a next-generation wireless cellular communication system. The network comprises a macro-cell with a macro BS and multiple pico-cells with their serving pico BSs. Apart from the transmitting radiations from the BSs in the downlink (DL), we are interested in the EMF exposure caused by handheld devices. For instance, the RF radiations emitting from cell phones and smartwatches are stronger nearer the users, resulting in near-field exposure, whereas the EMF transmission density from BS towers situated far from the users render far-field exposure. Likewise, increasing applications and use cases including but not limited to autonomous vehicles and smart homes/offices, etc., are extending their radiation footprint near humans. **Figure 1** demonstrates a strong radiation pattern near users in the case of voice users when compared with data users. In addition, we account for the performance degradation caused by the additive HWDs accumulating from the various blocks in nonideal RF transceivers. We propose a generalized digital communication system capable of transmitting nonuniformly distributed symbols (from a uniform bitstream using distribution matching) while using an appropriate receiver for optimal detection.

2.1 Radiation Exposure

The modeling and quantification of human exposure in a wireless cellular network are critical to facilitate the reduction efforts. Numerous studies have identified the essential parameters influencing this end exposure (Kuehn et al., 2019; Lou et al., 2021; Vermeeren et al., 2015a). The EMF exposure, quantified as the exposure index (EI), is primarily dictated by the network topology, environment, radio access technology, user scenarios, and service types (Kuehn et al., 2019). The EI can be written as the weighted sum of all branches in the chain of exposure (Lou et al., 2021).

$$\mathrm{EI} = \sum_{g}\sum_{p}\sum_{e}\sum_{r}\sum_{l}\sum_{s} f\left(\mathrm{SAR}^{\mathrm{UL}}, \alpha, \mathrm{SAR}^{\mathrm{DL}}, \varrho\right) \tag{1}$$

where the specific absorption rate (SAR), measured in W/kg, is the power absorbed per mass of the exposed tissue for a given period, with $\mathrm{SAR}^{\mathrm{UL}}$ and $\mathrm{SAR}^{\mathrm{DL}}$ indicating the normalized values of the UL- and DL-induced SARs when the mean transmit power $\alpha = 1\mathrm{W}$ and the mean received power density $\varrho = 1\mathrm{W/m}^2$, respectively. The EI is integrated over different age groups g (e.g., children, young people, adults, and seniors), user posture p (e.g., standing and sitting), environments e (e.g., indoor, outdoor, and commuting), radio access technology r (e.g., GSM, UMTS, Wi-Fi, 5G), layers l (macro, micro, pico, and femto), and service/usage types s (e.g., voice and data) (Tesanovic et al., 2014). We consider an exposure scenario of the next-generation cellular network in an indoor environment where the reference SAR is averaged over different population ages and postures, accommodating both data and voice usage types. The EI for both the UL and DL can be given by $\mathrm{EI} = \mathrm{EI}^{\mathrm{UL}} + \mathrm{EI}^{\mathrm{DL}}$, combining the DL exposure induced all day long by base stations/access points and the UL exposure incurred by individual wireless communication devices.

Contrary to the general perception, the SAR from the UL renders the dominant part instead of the one from DL with low ϱ (generally $\leq 10\mathrm{mW/m}^2$ according to FCC), given a significant distance between the transmitter and receiver. Thus, the exposure index (EI) metric in the presented scenario is dominated by the UL as $\mathrm{EI}(\alpha) = \mathrm{SAR}^{\mathrm{UL}}\alpha$, the reference whole body or localized SAR mainly depends on the required service and the posture (Vermeeren et al., 2015b; Lou et al., 2021).

2.2 Hardware-Impaired Signal Model

The nonlinear transfer functions of various transmitter RF stages, such as the digital-to-analog converter, band-pass filter, and high-power amplifier, result in additive distortion noise η_{t}, which is distributed as a zero-mean complex Gaussian random variable $\eta_{\mathrm{t}} \sim \mathcal{CN}(0, \kappa_{\mathrm{t}}, \tilde{\kappa}_{\mathrm{t}})$ with variance κ_{t} and pseudo-variance $\tilde{\kappa}_{\mathrm{t}}$. The complete statistical characterization requires pseudo-variance, in addition to the variance, accounting for the correlated and/or unequal power distribution among quadrature components of the general complex Gaussian random variable (Javed et al., 2017). Importantly, the value of pseudo-variance is limited by the variance as $|\tilde{\kappa}_{\mathrm{t}}| \leq \kappa_{\mathrm{t}}$ (Björnson et al., 2013; Schenk, 2008).

The Gaussian model for the aggregate residual RF distortions is based on various theoretical investigations, including the central limit theorem and measurement results after applying existing compensation schemes (Wenk, 2010; Zetterberg, 2011; Boulogeorgos et al., 2016; Xia et al., 2015; Suzuki et al., 2008; Studer et al., 2010; Duy et al., 2015; Björnson et al., 2014; and references therein). This can also be motivated analytically by the central limit theorem. The accumulative distortions raise the noise floor of the transmitted signal as $x_{\mathrm{tx}} = x_m + \eta_{\mathrm{t}}$, where x_m is the single-carrier band-pass–modulated signal taken from M-ary QAM, M-ary PSK, or M-ary PAM constellation with a probability mass function $p_m \triangleq p_X(x_m)$, rendering the transmission probability of symbol x_m, and $\mathbf{p} \triangleq [p_1, p_2, \ldots, p_M]$. Let us define the set that includes all the possible symbol distributions as

$$\mathbb{S} = \left\{ \mathbf{p}\colon \mathbf{p} = [p_1, p_2, \ldots, p_M], \sum_{j=1}^{M} p_j = 1, p_j \geq 0, \forall j \in \{1, 2, \ldots, M\} \right\}.$$

The information-bearing signal is transmitted with an average power α and received under an additive white Gaussian noise (AWGN) condition and receiver distortions $\eta_{\mathrm{r}} \sim \mathcal{CN}(0, \alpha\kappa_{\mathrm{r}}, \alpha\tilde{\kappa}_{\mathrm{r}})$. These distortions result from the nonlinear transfer function of low-noise amplifier, band-pass filters, image rejection low-pass filter, and analog-to-digital converter at the receiver. Thus, the received signal in point-to-point (P2P) communication under improper HWD can be modeled as

$$y = \sqrt{\alpha}x_m + \sqrt{\alpha}\eta + w; \quad m = 1, 2, \ldots, M \tag{2}$$

where $w \sim \mathcal{CN}(0, \sigma_w^2, 0)$ is the thermal noise, and the aggregate effect of transceiver distortions is represented by $\eta \sim \mathcal{CN}(0, \kappa, \tilde{\kappa})$, $\kappa = \kappa_{\mathrm{t}} + \kappa_{\mathrm{r}}$ and $\tilde{\kappa} = \tilde{\kappa}_{\mathrm{t}} + \tilde{\kappa}_{\mathrm{r}}$. Interestingly, the generalized impropriety characterization assists in accurate system modeling, rigorous performance analysis, and appropriate signaling design. Interested readers can study the work by Javed et al. (2020) for the details of statistical impropriety characterization.

2.3 Noise Distribution and Optimal Receiver

Considering the aggregate noise $z = \sqrt{\alpha}\eta + w$ distributed as $z \sim CN(0, \alpha\kappa + \sigma_w^2, \alpha\tilde{\kappa})$ where in-phase z_{I} and quadrature-phase z_{Q} noise components are distributed with the respective variances as

$$\sigma_I^2 = \left(\alpha(\kappa + \Re(\tilde{\kappa})) + \sigma_w^2\right)\Big/2, \tag{3}$$

$$\sigma_Q^2 = \left(\alpha(\kappa - \Re(\tilde{\kappa})) + \sigma_w^2\right)\Big/2, \tag{4}$$

These individual variances are obtained by simultaneously solving the equations of variance, that is, $\mathbb{E}\{|z|^2\} = \sigma_I^2 + \sigma_Q^2$ and pseudo-variance $\mathbb{E}\{z^2\} = \sigma_I^2 - \sigma_Q^2 + 2ir_{z_I z_Q}$. Thus, the correlation $r_{z_I z_Q} = \alpha\Im(\tilde{\kappa})/2$ defines the correlation coefficient ρ_z between z_{I} and z_{Q} as

$$\rho_z = \frac{r_{z_I z_Q}}{\sigma_I \sigma_Q} = \frac{\alpha\Im(\tilde{\kappa})}{\sqrt{\left(\alpha\kappa + \sigma_w^2\right)^2 - \left(\alpha\Re(\tilde{\kappa})\right)^2}}. \tag{5}$$

Unequal power distribution among the quadrature noise components and nontrivial correlation coefficient marks the improper nature of aggregate additive distortions. Given the nonuniform symbol probabilities and improper noise, we propose a maximum *a posterior* (MAP) detector for the optimal detection as opposed to the conventional minimum Euclidean or maximum likelihood (ML) detectors (Javed et al., 2021). Thus, the detection criterion is given by

$$\hat{m}_{\mathrm{PS}} = \underset{1\le m\le M}{\operatorname{argmax}} \quad p_X(x_m) f_{Y_\mathrm{I},Y_\mathrm{Q}|X}(y_\mathrm{I}, y_\mathrm{Q}|x_m), \tag{6}$$

where $f_{Y_\mathrm{I},Y_\mathrm{Q}|X}(y_\mathrm{I}, y_\mathrm{Q}|x_m)$ is the conditional Gaussian probability density function (PDF) of y given that x_m is derived using Javed et al. (2020, eq. 43)

$$f_{Y_\mathrm{I},Y_\mathrm{Q}|X}(y_\mathrm{I}, y_\mathrm{Q}|x_m) = \frac{1}{2\pi\sigma_\mathrm{I}\sigma_\mathrm{Q}\sqrt{1-\rho_z^2}}$$

$$\exp\left\{\frac{-1}{2(1-\rho_z^2)}\left[\frac{\left(y_\mathrm{I}-\sqrt{\alpha}\,\Re(x_m)\right)^2}{\sigma_\mathrm{I}^2}+\frac{\left(y_\mathrm{Q}-\sqrt{\alpha}\,\Im(x_m)\right)^2}{\sigma_\mathrm{Q}^2}+\right.\right.$$
$$\left.\left.-\frac{2\rho_z\left(y_\mathrm{I}-\sqrt{\alpha}\,\Re(x_m)\right)\left(y_\mathrm{Q}-\sqrt{\alpha}\,\Im(x_m)\right)}{\sigma_\mathrm{I}\sigma_\mathrm{Q}}\right]\right\}. \tag{7}$$

3 ERROR PROBABILITY ANALYSIS

In this section, we derive the symbol error probability P_s for a system transmitting M-ary–modulated symbols with prior probabilities p_m and subjected to HWD using the union-bound and pairwise error probability as follows:

$$P_s \le \sum_{m=0}^{M-1}\sum_{n\neq m} P_m \Pr(x_m \to x_n|x_m). \tag{8}$$

The pairwise error probability, for receiving an erroneous symbol x_m given x_n was transmitted, can be derived using the following MAP rule:

$$\Pr(x_m \to x_n|x_m) = \Pr\Big\{P_m f_{Y_I,Y_Q}(y_I, y_Q|x_m)$$
$$\le P_n f_{Y_I,Y_Q}(y_I, y_Q|x_n)\Big\}. \tag{9}$$

Using **(7)** and few simplifications, we get the following bit error probability as

$$P_\mathrm{b} \le \mathrm{P}_\mathrm{b}^{\mathrm{UB}}(M,\alpha,\mathbf{p}) \triangleq \frac{1}{\log_2(M)}\sum_{m=1}^{M}\sum_{\substack{n=1\\ n\neq m}}^{M} p_m \mathcal{Q}\left(\beta_{mn}(\alpha)\ln\left(\frac{p_m}{p_n}\right)+\frac{1}{2\beta_{mn}(\alpha)}\right), \tag{10}$$

where β_{mn} is defined as

$$\beta_{mn}(\alpha) \triangleq \sqrt{\frac{\alpha^2\left(\kappa^2-\Re(\tilde{\kappa})^2-\Im(\tilde{\kappa})^2\right)+2\alpha\kappa\sigma_w^2+\sigma_w^4}{\alpha^2\wp_{\mathrm{mn}}+\alpha\left(\xi_{mnI}^{\ 2}+\xi_{mnQ}^{\ 2}\right)2\sigma_w^2}}, \tag{11}$$

with $\wp_{\mathrm{mn}} = 2\xi_{mnI}^{\ 2}(\kappa-\Re(\tilde{\kappa}))+2\xi_{mnQ}^{\ 2}(\kappa+\Re(\tilde{\kappa}))-4\Im(\tilde{\kappa})\xi_{mnI}\xi_{mnQ}$, while $\xi_{mn} = d_{mn} = x_m - x_n$ represents the distance between the m^{th} and n^{th} symbols.

4 PROBLEM FORMULATION AND OPTIMIZATION

We propose a PS scheme, as a possible form of AS schemes, to effectively mitigate the drastic effects of additive distortions while transmitting with minimum power to minimize the EMF exposure. To this end, we employ a higher-order M_{nu} probabilistically shaped quadrature amplitude modulation (QAM) offering more degrees of freedom and adaptive rates. The optimization problem targets the joint design of the transmit power and symbol probabilities which minimize the exposure index while maintaining a throughput quality constraint. Assuming that the set includes all possible values of α as $\mathbb{A} = \{\alpha: 0 \le \alpha \le \alpha_{\max}\}$, we can formulate the optimization problem as

$$\mathbf{P1}: \quad \underset{\alpha\in\mathbb{A},\mathbf{p}\in\mathbb{S}}{\text{minimize}}\ \mathrm{EI}(\alpha) \tag{12a}$$

$$\text{subject to} \quad \sum_{m=1}^{M_{\mathrm{nu}}} |x_m|^2 p_m \le 1, \tag{12b}$$

$$\left(1-\mathrm{P}_\mathrm{b}^{\mathrm{UB}}(M_{\mathrm{nu}},\alpha,\mathbf{p})\right)\mathrm{H}(\mathbf{p}) \ge \mathcal{T}_\mathrm{u}, \tag{12c}$$

where $\mathcal{T}_\mathrm{u} = (1-\mathrm{P}_\mathrm{b}^{\mathrm{UB}}(M_\mathrm{u},\alpha_{\max},\mathbf{p}_\mathrm{u}))\log_2(M_\mathrm{u})$ is the throughput of the constellation with maximum power transmission. Moreover, (12b) and (12c) represent the average power and throughput QoS constraints, respectively. In addition, $\mathrm{H}(\mathbf{p})$ is the source entropy, which represents the transmitted rate in terms of bits per symbol per channel use and is defined as

$$\mathrm{H}(\mathbf{p}) \triangleq \sum_{m=1}^{M_{\mathrm{nu}}} -p_m \log_2(p_m). \tag{13}$$

The joint optimization problem is challenging due to the non-convex constraints. Therefore, we adopt an alternate optimization approach to iteratively solve the transmit power and symbol probabilities using the subproblems (14) and (21), respectively. The alternate optimization Algorithm 1 begins with some initial feasible points $\mathbf{p}^{(j)}$ and $\alpha^{(j)}$ and evaluates $\mathrm{EI}(\alpha^{(j)})$ for a reference benchmark. Then, it finds a feasible solution of **P1(a)**, that is, $\mathbf{p}^{(j\star)}$ that satisfies (12b) and (12c). Given a probability mass function (PMF) $\mathbf{p}^{(j\star)}$, we optimize **P1(b)** to minimize the exposure index obtaining optimal $\alpha^{(j\star)}$, which is updated to attain initial points for the next iteration. This iterative process continues until reaching an acceptable tolerance δ. Consequently, the solution parameters yield a suitable PMF and transmission power, which render a minimum exposure index while maintaining a throughput QoS.

Algorithm 1. Alternate Optimization

Initialize $j \leftarrow 0$, $\epsilon \leftarrow \infty$ and **Set** tolerance δ
Choose feasible starting points $\mathbf{p}^{(j)}$ and $\alpha^{(j)}$.
Evaluate $\mathrm{EI}\left(\alpha^{(j)}\right)$.
while $\epsilon \ge \delta$ **do**
  Solve **P1(a)** with given $\alpha^{(j)}$ and initial point $\mathbf{p}^{(j)}$ to obtain a feasible solution $\mathbf{p}^{(j*)}$
  Solve **P1(b)** given $\mathbf{p}^{(j*)}$ to obtain $\alpha^{(j*)}$
  $\mathbf{p}^{(j+1)} \leftarrow \mathbf{p}^{(j*)}$ and $\alpha^{(j+1)} \leftarrow \alpha^{(j*)}$
  Evaluate $\mathrm{EI}\left(\alpha^{(j+1)}\right)$
  Update $\epsilon \leftarrow \left\|\mathrm{EI}\left(\alpha^{(j+1)}\right) - \mathrm{EI}\left(\alpha^{(j)}\right)\right\|$
  $j \leftarrow j+1$
end while
Solution parameters: $\mathbf{p}^* \leftarrow \mathbf{p}^{(j+1)}$ and $\alpha^* \leftarrow \alpha^{(j+1)}$
Objective function: $\mathrm{EI}\left(\alpha^{(*)}\right)$

$$\mathbf{P1}(\mathbf{a}): \quad \underset{\mathbf{p}\in\mathbb{S}}{\text{find}}\ \mathbf{p} \tag{14a}$$

$$\text{which satisfies} \quad (12b) \text{ and} \tag{14b}$$

$$1 - \mathrm{P}_{\mathrm{b}}^{\mathrm{UB}}\left(M_{\mathrm{nu}}, \alpha, \mathbf{p}\right) \geq \mathcal{T}_{\mathrm{u}}/\mathrm{H}\left(\mathbf{p}\right), \tag{14c}$$

The problem **P1(a)** is a non–convex optimization problem due to the constraint (14*c*). Interestingly, $1/\mathrm{H}(\mathbf{p})$ is convex, as the second derivative is always positive (see **Appendix**). However, the bit error probability is a non–convex function in $\mathbf{p}$. Therefore, we tackle this challenge using the successive convex approximation approach based on the Taylor series approximation of the bit error probability. The first-order Taylor series approximation of a function $f(x)$ around a point $x^{(k)}$ is given as

$$\tilde{f}\left(x, x^{(k)}\right) \approx f\left(x^{(k)}\right) + \nabla_x f\left(x^{(k)}\right)\left(x - x^{(k)}\right). \tag{15}$$

Thus, we need to compute $\nabla_{\mathbf{p}} \mathrm{P}_{\mathrm{b}}^{\mathrm{UB}}\left(M_{\mathrm{nu}}, \alpha, \mathbf{p}\right)$ and evaluate it as $\mathbf{p}^{(k)}$.

$$\nabla_{\mathbf{p}} \mathrm{P}_{\mathrm{b}}^{\mathrm{UB}}\left(M_{\mathrm{nu}}, \alpha, \mathbf{p}\right) = \left[\frac{\partial \mathrm{P}_{\mathrm{b}}^{\mathrm{UB}}}{\partial p_1} \quad \frac{\partial \mathrm{P}_{\mathrm{b}}^{\mathrm{UB}}}{\partial p_2} \quad \cdots \quad \frac{\partial \mathrm{P}_{\mathrm{b}}^{\mathrm{UB}}}{\partial p_{M_{\mathrm{nu}}}}\right]. \tag{16}$$

In order to compute $\partial \mathrm{P}_{\mathrm{b}}^{\mathrm{UB}}/\partial p_t$, we rewrite (10) as

$$\mathrm{P}_{\mathrm{b}}^{\mathrm{UB}}\left(M_{\mathrm{nu}}, \alpha, \mathbf{p}\right) = \frac{1}{\log_2\left(M_{\mathrm{nu}}\right)} \sum_{m=1}^{M_{\mathrm{nu}}} \sum_{\substack{n=1 \\ n \neq m}}^{M_{\mathrm{nu}}} p_m \int_{\Omega_{mn}}^{\infty} \frac{e^{-\frac{u^2}{2}}}{\sqrt{2\pi}} du, \tag{17}$$

where Ω_{mn} is defined as

$$\Omega_{mn} = \beta_{mn} \ln\left(\frac{p_m}{p_n}\right) + \frac{1}{2\beta_{mn}}. \tag{18}$$

Applying the Leibniz integral rule on **(17)** yields the following partial derivative:

$$\frac{\partial \mathrm{P}_{\mathrm{b}}^{\mathrm{UB}}}{\partial p_t} \leq \frac{1}{\log_2\left(M_{\mathrm{nu}}\right)} \sum_{\substack{n=1, \\ n \neq t, \\ m=t}}^{M_{\mathrm{nu}}} \left(\mathcal{Q}\left(\Omega_{mn}\right) - \frac{\beta_{mn}}{\sqrt{2\pi}} e^{-\frac{\Omega_{mn}^2}{2}}\right) + \frac{1}{\log_2\left(M_{\mathrm{nu}}\right)} \sum_{\substack{m=1, \\ m \neq t, \\ n=t}}^{M_{\mathrm{nu}}} \frac{\beta_{mn} p_m}{\sqrt{2\pi} p_n} e^{-\frac{\Omega_{mn}^2}{2}}. \tag{19}$$

Now, $\mathrm{P}_{\mathrm{b}}^{\mathrm{UB}}\left(M_{\mathrm{nu}}, \alpha, \mathbf{p}\right)$ can be approximated from **Eqs. 15**, **16**, **19** using first-order Taylor series expansion around an initial probability vector $\mathbf{p}^{(k)}$ as

$$\tilde{\mathrm{P}}_{\mathrm{b}}^{\mathrm{UB}}\left(M_{\mathrm{nu}}, \alpha, \mathbf{p}, \mathbf{p}^{(k)}\right) \triangleq \mathrm{P}_{\mathrm{b}}^{\mathrm{UB}}\left(M_{\mathrm{nu}}, \alpha, \mathbf{p}^{(k)}\right) + \nabla_{\mathbf{p}} \mathrm{P}_{\mathrm{b}}^{\mathrm{UB}}\left(M_{\mathrm{nu}}, \alpha, \mathbf{p}^{(k)}\right)\left(\mathbf{p} - \mathbf{p}^{(k)}\right). \tag{20}$$

Conclusively, we can solve **P1 (a)** by replacing $\mathrm{P}_{\mathrm{b}}^{\mathrm{UB}}\left(M_{\mathrm{nu}}, \alpha, \mathbf{p}\right)$ in **(14c)** with its Taylor series approximation $\tilde{\mathrm{P}}_{\mathrm{b}}^{\mathrm{UB}}\left(M_{\mathrm{nu}}, \alpha, \mathbf{p}, \mathbf{p}^{(k)}\right)$ and solving the resultant convex feasibility problem iteratively using the well-known successive convex approximation approach (Liu et al., 2019). On the other hand, we solve **P1 (b)** for a given PMF to obtain an optimal $\alpha^{\star}$ which minimizes the EMF exposure.

$$\mathbf{P1\,(b)}: \quad \underset{\alpha \in \mathbb{A}}{\text{minimize}} \ \mathrm{EI}\left(\alpha\right) \tag{21a}$$

$$\text{subject to} \quad (12c) \tag{21b}$$

Intuitively, the throughput of probabilistically shaped M_{nu}-ary QAM is an increasing function of α because $\mathrm{P}_{\mathrm{b}}^{\mathrm{UB}}\left(M_{\mathrm{nu}}, \alpha, \mathbf{p}\right)$ is a decreasing function of α. Therefore, the solution to the problem **P1 (b)** is simply obtained by solving the inequality constraint with equality as

$$\mathrm{P}_{\mathrm{b}}^{\mathrm{UB}}\left(M_{\mathrm{nu}}, \alpha, \mathbf{p}\right) = 1 - \mathcal{T}_{\mathrm{u}}/\mathrm{H}\left(\mathbf{p}\right) \tag{22}$$

The root of the nonlinear equation $\Upsilon(\alpha) = \mathrm{P}_{\mathrm{b}}^{\mathrm{UB}}\left(M_{\mathrm{nu}}, \alpha, \mathbf{p}\right) + \mathcal{T}_{\mathrm{u}}/\mathrm{H}\left(\mathbf{p}\right) - 1$ can be obtained using the Newton–Raphson method, which begins with an initial guess $\alpha^{(j)}$ and updates it with every iteration as explained by Kelley (2003):

$$\alpha^{(j+1)} = \alpha^{(j)} - \frac{\Upsilon\left(\alpha^{(j)}\right)}{\Upsilon'\left(\alpha^{(j)}\right)}. \tag{23}$$

It is worthy to note that $\Upsilon'(\alpha^{(j)}) \neq 0$ and is computed from **(17)** as

$$\Upsilon'\left(\alpha\right) = \frac{1}{\log_2\left(M_{\mathrm{nu}}\right)} \sum_{m=1}^{M_{\mathrm{nu}}} \sum_{\substack{n=1 \\ n \neq m}}^{M_{\mathrm{nu}}} p_m \frac{e^{-\Omega_{mn}^2/2}}{\sqrt{2\pi}} \left(\frac{1}{2\beta_{mn}^2} - \ln\left(\frac{p_m}{p_n}\right)\right) \frac{\partial \beta_{mn}}{\partial \alpha}, \tag{24}$$

where $\frac{\partial \beta_{mn}}{\partial \alpha}$ is expressed as

$$\frac{\partial \beta_{mn}}{\partial \alpha} = \frac{1}{2} \sqrt{\frac{\alpha^2 \wp_{\mathrm{mn}} + \alpha\left(\xi_{mnI}^{\ 2} + \xi_{mnQ}^{\ 2}\right) 2\sigma_w^2}{\alpha^2\left(\kappa^2 - \Re\left(\tilde{\kappa}\right)^2 - \Im\left(\tilde{\kappa}\right)^2\right) + 2\alpha\kappa\sigma_w^2 + \sigma_w^4}} \ \mathrm{x} \tag{25}$$

$$\left\{\frac{2\alpha\left(\kappa^2 - \Re\left(\tilde{\kappa}\right)^2 - \Im\left(\tilde{\kappa}\right)^2\right) + 2\kappa\sigma_w^2}{\alpha^2 \wp_{\mathrm{mn}} + \alpha\left(\xi_{mnI}^{\ 2} + \xi_{mnQ}^{\ 2}\right) 2\sigma_w^2} - \frac{\psi\left(2\alpha\wp_{\mathrm{mn}} + \left(\xi_{mnI}^{\ 2} + \xi_{mnQ}^{\ 2}\right) 2\sigma_w^2\right)}{\left(\alpha^2 \wp_{\mathrm{mn}} + \alpha\left(\xi_{mnI}^{\ 2} + \xi_{mnQ}^{\ 2}\right) 2\sigma_w^2\right)^2}\right\} \tag{26}$$

with $\psi = \alpha^2\left(\kappa^2 - \Re\left(\tilde{\kappa}\right)^2 - \Im\left(\tilde{\kappa}\right)^2\right) + 2\alpha\kappa\sigma_w^2 + \sigma_w^4$. The process is repeated until the desired criterion is met in terms of precision, that is, $\Upsilon(\alpha)$ becomes acceptably small and the change α is lesser than the predefined limit or maximum number of iterations.

5 NUMERICAL RESULTS

In this section, we present some numerical results to quantify the EMF exposure caused by the proposed PS scheme instead of conventional no-shaping (NS). We consider an indoor active user in the next-generation cellular network suffering from improper HWDs. We assume $\kappa \in \{0, 1\}$, $\rho = 0.9$, $\sigma_w^2 = 1$, $M_{\mathrm{u}} = 8$ – QAM, and $M_{\mathrm{nu}} = 16$ – QAM unless specified otherwise. The reference whole-body SAR values are taken from the study by Vermeeren et al. (2015a, Table 27), which were computed using 3D EM-simulation platforms based on the finite difference time domain and finite integration technique method. For instance, the whole-body $\mathrm{SAR}^{\mathrm{ref}}$ for a standing adult is 0.0053 and while sitting is 0.0047. On the other hand, for a child it is 0.015 and 0.014, respectively, for the uplink voice communication at the 2.6-GHz frequency band. In number results, we take the average reference SAR weighted by the number of users in each category along with their respective postures. In particular, we consider $\mathrm{SAR}^{\mathrm{ref}} = 41 \times 10^{-4}$ W/Kg for data users and $\mathrm{SAR}^{\mathrm{ref}} = 63 \times 10^{-4}$ W/Kg for voice users per unit power (Ibraiwish et al., 2022). Evidently, the SAR reference value

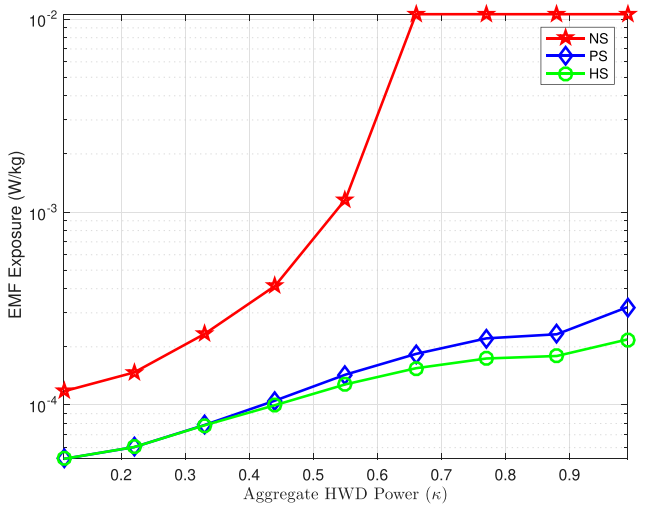

FIGURE 2 | Exposure index [W/kg] versus HWD power when NS transmits with α_{max}.

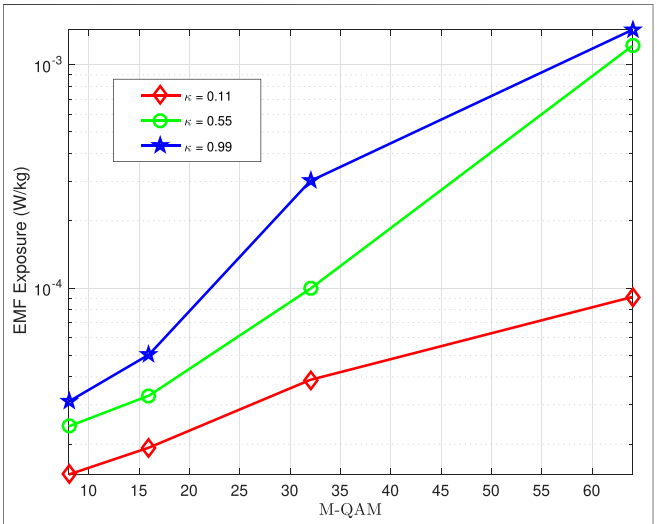

FIGURE 3 | Exposure index [W/kg] versus modulation order.

of voice users is higher than that of data users because the voice users are expected to keep their mobile phones near their brains.

At first, we investigate the EMF exposure of a single active user for a range of HWD levels. We present the comparison between the traditional NS scheme employing M_{u} − QAM and the proposed PS scheme employing M_{nu} − QAM. For a fair comparison, we minimize the exposure index of M_{u} − QAM with uniform distribution $\mathbf{p}_u$ (NS) scheme to ensure a throughput threshold of $\mathcal{T}_0 = 2.997$ bits/sec, that is,

$$\mathbf{P2}(\mathbf{a}): \quad \underset{\alpha_{\mathrm{u}} \in \mathbb{A}}{\text{minimize}} \ \mathrm{EI}(\alpha_{\mathrm{u}}) \tag{27a}$$

$$\text{subject to} \quad \left(1 - \mathrm{P}_{\mathrm{b}}^{\mathrm{UB}}\left(M_{\mathrm{u}}, \alpha, \mathbf{p}_u\right)\right)\log_2\left(M_{\mathrm{u}}\right) \geq \mathcal{T}_0, \tag{27b}$$

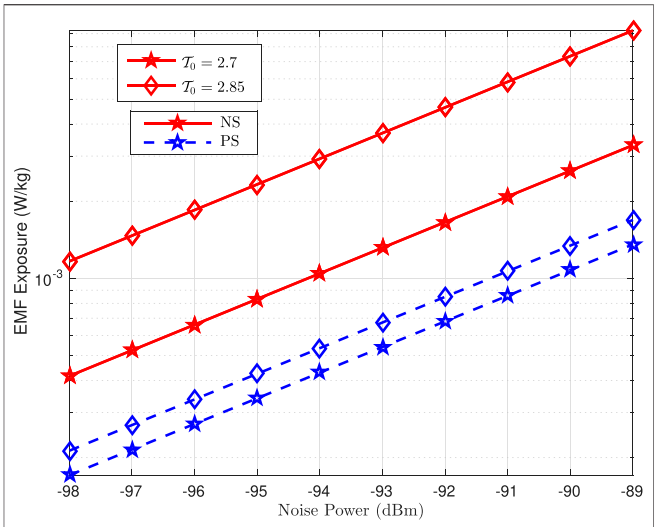

FIGURE 4 | Exposure index [W/kg] versus noise variance.

The simulation results provide insights into the exposure index of non-shaping versus probabilistic shaping for a range of HWDs to achieve a target throughput, as shown in **Figure 2**. Evidently, they reveal the superiority of employing PS to successfully limit the EMF exposure while maintaining the QoS in terms of throughput. The advantage of PS over NS is particularly prominent for higher distortion levels. Moreover, we move a step further to investigate the performance of the HS scheme with M_{nu} − QAM employing an aggregate of GS and PS as detailed in the study by Javed et al. (2021). Interestingly, HS reduces the EMF exposure for higher distortion levels, but the gain is insignificant given the added complexity in designing GS and PS parameters. Conclusively, PS is the preferred choice as it can reduce EMF exposure up to 98% with affordable complexity.

Next, we study the impact of varying the modulation order for three different distortion levels on the EMF exposure as shown in **Figure 3**. We assumed a modulation order M_{nu} ranging from 8-QAM to 64-QAM for the proposed PS. Noticeably, the increasing modulation order increases the EMF exposure for all HWD levels, that is, least, medium, and high distortion levels, however, at different paces. Intuitively, more transmit power is required to meet the QoS constraint in a highly distorted system instead of the least distorted system, which advocates a considerable EMF exposure of higher distortion levels.

Similarly, we analyzed the benefits of PS over NS for a range of noise variance (−98dBm to −89dBm) for two different target throughputs, that is, $\mathcal{T}_0 = 2.7$ bits/sec and $\mathcal{T}_0 = 2.85$ bits/sec. We can observe a 55 and 81.82% reduction in EMF exposure at −98dBm for the target threshold rates of 2.7 and 2.85 bits per sec per channel, respectively, with PS over NS as shown in **Figure 4**. Intuitively, PS outperforms NS for the entire range of noise variance in decreasing the EMF exposure on a user.

6 CONCLUSION

Throughout this study, we highlight the significance of employing probabilistic shaping (PS) to mitigate the drastic effects of improper hardware distortions and effectively reduce the user's EMF exposure while maintaining a target threshold. The numerical results reveal up to a 98% reduction in the exposure index with the help of PS as compared to the conventional NS. Further investigation demonstrates a minor gain with HS over PS with significant added complexity. Thus, we conclude that mere PS is the preferred choice to reduce the exposure index, given a trade-off between lowering the EI and increasing computational complexity.

DATA AVAILABILITY STATEMENT

The original contributions presented in the study are included in the article/Supplementary Material, further inquiries can be directed to the corresponding author.

AUTHOR CONTRIBUTIONS

The study was conducted as a collaboration among all authors. AE conceived the work. The manuscript was mainly drafted by SJ and was revised and approved by all co-authors.

REFERENCES

Bhushan, N., Junyi Li, J., Malladi, D., Gilmore, R., Brenner, D., Damnjanovic, A., et al. (2014). Network Densification: the Dominant Theme for Wireless Evolution into 5G. *IEEE Commun. Mag.* 52, 82–89. doi:10.1109/mcom.2014.6736747

Björnson, E., Hoydis, J., Kountouris, M., and Debbah, M. (2014). Massive MIMO Systems with Non-ideal Hardware: Energy Efficiency, Estimation, and Capacity Limits. *IEEE Trans. Inf. Theor.* 60, 7112. doi:10.1109/TIT.2014.2354403

Björnson, E., Matthaiou, M., and Debbah, M. (2013). A New Look at Dual-Hop Relaying: Performance Limits with Hardware Impairments. *IEEE Trans. Commun.* 61, 4512. doi:10.1109/TCOMM.2013.100913.13

Boulogeorgos, A.-A. A., Chatzidiamantis, N. D., and Karagiannidis, G. K. (2016). Energy Detection Spectrum Sensing under RF Imperfections. *IEEE Trans. Commun.* 64, 2754–2766. doi:10.1109/tcomm.2016.2561294

Buchner, K., and Rivasi, M. (2020). *The International Commission on Non-ionizing Radiation protection: Conflicts of Interest, Corporate Capture and the Push for 5G*. Brussels: European Parliament – Michèle Rivasi (Europe Écologie) and Klaus Buchner (Ökologisch-Demokratische Partei).

Chiaraviglio, L., Elzanaty, A., and Alouini, M.-S. (2021). Health Risks Associated with 5G Exposure: A View from the Communications Engineering Perspective. *IEEE Open J. Commun. Soc.* 2, 2131–2179. doi:10.1109/OJCOMS.2021.3106052

Duy, T. T., Duong, T. Q., da Costa, D. B., Bao, V. N. Q., and Elkashlan, M. (2015). Proactive Relay Selection with Joint Impact of Hardware Impairment and Co-channel Interference. *IEEE Trans. Commun.* 63, 1594–1606. doi:10.1109/tcomm.2015.2396517

Elzanaty, A., Chiaraviglio, L., and Alouini, M.-S. (2021). 5G and EMF Exposure: Misinformation, Open Questions, and Potential Solutions. *Front. Comms. Net.* 2, 5. doi:10.3389/frcmn.2021.635716

Elzanaty, A. M., and Alouini, M.-S. (2022). Communicating over a Free-Space Optical Channel Using Distribution Matching. *US Patent App* 17/357, 450.

Group, I. W. (2013). Non-ionizing Radiation, Part 2: Radiofrequency Electromagnetic fields. *IARC Monogr. Eval. Carcinog Risks Hum.* 102, 1.

Ibraiwish, H., Elzanaty, A., Al-Badarneh, Y. H., and Alouini, M.-S. (2022). EMF-aware Cellular Networks in RIS-Assisted Environments. *IEEE Commun. Lett.* 26, 123–127. doi:10.1109/LCOMM.2021.3120688

Javed, S., Amin, O., Ikki, S. S., and Alouini, M.-S. (2017). Asymmetric Hardware Distortions in Receive Diversity Systems: Outage Performance Analysis. *IEEE Access* 5, 4492–4504. doi:10.1109/access.2017.2672543

Javed, S., Amin, O., Shihada, B., and Alouini, M.-S. (2020). A Journey from Improper Gaussian Signaling to Asymmetric Signaling. *IEEE Commun. Surv. Tutorials* 22, 1539–1591. doi:10.1109/COMST.2020.2989626

Javed, S., Amin, O., Shihada, B., and Alouini, M.-S. (2019). Improper Gaussian Signaling for Hardware Impaired Multihop Full-Duplex Relaying Systems. *IEEE Trans. Commun.* 67, 1858–1871. doi:10.1109/tcomm.2018.2884986

Javed, S., Elzanaty, A., Amin, O., Shihada, B., and Alouini, M.-S. (2021). When Probabilistic Shaping Realizes Improper Signaling for Hardware Distortion Mitigation. *IEEE Trans. Commun.* 69, 5028–5042. doi:10.1109/tcomm.2021.3074978

Kelley, C. T. (2003). *Solving Nonlinear Equations with Newton's Method*. Philadelphia, PA: Society for Industrial and Applied Mathematics (SIAM), University City Science Center.

Kuehn, S., Pfeifer, S., Kochali, B., Kuster, N., and Bern, C. (2019). Modelling of Total Exposure in Hypothetical 5G mobile Networks for Varied Topologies and User Scenarios. *Final Rep. Project CRR* 816.

Latva-aho, M., Leppänen, K., Clazzer, F., and Munari, A. (2020). *Key Drivers and Research Challenges for 6G Ubiquitous Wireless Intelligence*. Oulu: 6G Flagship, University of Oulu.

Liu, A., Lau, V. K. N., and Kananian, B. (2019). Stochastic Successive Convex Approximation for Non-convex Constrained Stochastic Optimization. *IEEE Trans. Signal. Process.* 67, 4189–4203. doi:10.1109/tsp.2019.2925601

Lou, Z., Elzanaty, A., and Alouini, M.-S. (2021). Green Tethered UAVs for EMF-Aware Cellular Networks. *IEEE Trans. Green. Commun. Netw.* 5, 1697–1711. doi:10.1109/TGCN.2021.3102086

Matalatala, M., Deruyck, M., Tanghe, E., Martens, L., and Joseph, W. (2018). "Optimal Low-Power Design of a Multicell Multiuser Massive MIMO System at 3.7 GHz for 5G Wireless Networks," in *Wireless Communications and Mobile Computing 2018*. doi:10.1155/2018/9796784

National Toxicology Program (2018a). Toxicology and Carcinogenesis Studies in Hsd: Sprague Dawley SD Rats Exposed to Whole-Body Radio Frequency Radiation at a Frequency (900 MHz) and Modulations (GSM and CDMA) Used by Cell Phones. *Tech. rep., NTO* 595, 1–446. doi:10.22427/NTP-TR-595

National Toxicology Program (2018b). Toxicology and Carcinogenesis Studies in B6C3F1/N Mice Exposed to Whole-Body Radio Frequency Radiation at a Frequency (1,900 MHz) and Modulations (GSM and CDMA) Used by Cell Phones. *Tech. rep., NTO* 596, 1–305. doi:10.22427/NTP-TR-596

Santamaria, I., Crespo, P., Lameiro, C., and Schreier, P. (2018). Information-theoretic Analysis of a Family of Improper Discrete Constellations. *Entropy* 20, 45. doi:10.3390/e20010045

Schenk, T. (2008). *RF Imperfections in High-Rate Wireless Systems: Impact and Digital Compensation*. Springer Dordrecht.

Studer, C., Wenk, M., and Burg, A. (2010). "MIMO Transmission with Residual Transmit-RF Impairments," in *Proc. Int. ITG Workshop on Smart Antennas (WSA)* (Bremen, Germany: IEEE), 189. doi:10.1109/wsa.2010.5456453

Suzuki, H., Thi Van Anh Tran, T. V. A., Collings, I. B., Daniels, G., and Hedley, M. (2008). Transmitter Noise Effect on the Performance of a MIMO-OFDM Hardware Implementation Achieving Improved Coverage. *IEEE J. Select. Areas Commun.* 26, 867–876. doi:10.1109/jsac.2008.080804

Tesanovic, M., Conil, E., De Domenico, A., Aguero, R., Freudenstein, F., Correia, L. M., et al. (2014). The LEXNET Project: Wireless Networks and EMF: Paving the Way for Low-EMF Networks of the Future. *IEEE Vehicular Techn. Mag.* 9, 20. doi:10.1109/MVT.2014.2312272

Vermeeren, G., Plets, D., Joseph, W., Martens, L., Oliveira, C., Sebastião, D., et al. (2015a). Low EMF Exposure Future Networks D2. 8 Global Wireless Exposure Metric Definition. *Tech. Rep.*

Vermeeren, G., Plets, D., Joseph, W., Martens, L., Oliveira, C., Sebastião, D., et al. (2015b). Low EMF Exposure Future Networks D2. 8 Global Wireless Exposure Metric Definition. *Tech. rep., LEXNET Project Deliverable* 2, 1–66.

Vornoli, A., Falcioni, L., Mandrioli, D., Bua, L., and Belpoggi, F. (2019). The Contribution of *In Vivo* Mammalian Studies to the Knowledge of Adverse

Effects of Radiofrequency Radiation on Human Health. *Ijerph* 16, 3379. doi:10.3390/ijerph16183379

Wan, L., Guo, Z., Wu, Y., Bi, W., Yuan, J., Elkashlan, M., et al. (2018). 4G\/5G Spectrum Sharing: Efficient 5G Deployment to Serve Enhanced Mobile Broadband and Internet of Things Applications. *IEEE Veh. Technol. Mag.* 13, 28–39. doi:10.1109/MVT.2018.2865830

Wenk, M. (2010). *MIMO-OFDM-testbed: Challenges, Implementations, and Measurement Results*. Zurich: ETH Zurich.

Wilbourn, J., Haroun, L., Heseltine, E., Kaldor, J., Partensky, C., and Vainio, H. (1986). Response of Experimental Animals to Human Carcinogens: an Analysis Based upon the IARC Monographs Programme. *Carcinogenesis* 7, 1853–1863. doi:10.1093/carcin/7.11.1853

Xia, X., Zhang, D., Xu, K., Ma, W., and Xu, Y. (2015). Hardware Impairments Aware Transceiver for Full-Duplex Massive MIMO Relaying. *IEEE Trans. Signal. Process.* 63, 6565–6580. doi:10.1109/tsp.2015.2469635

Zetterberg, P. (2011). Experimental Investigation of TDD Reciprocity-Based Zero-Forcing Transmit Precoding. *EURASIP J. Adv. Signal. Process.* 2011, 5. doi:10.1155/2011/137541

Conflict of Interest: The authors declare that the research was conducted in the absence of any commercial or financial relationships that could be construed as a potential conflict of interest.

APPENDIX

Appendix A: Proof of Convexity

The first- and second-order derivatives of $1/\mathrm{H}(\mathbf{p})$ are given as

$$\nabla_{\mathbf{p}}\left(1/\mathrm{H}(\mathbf{p})\right) = -\mathrm{H}'(\mathbf{p})\Big/\left[\mathrm{H}(\mathbf{p})\right]^2 \tag{28}$$

$$\nabla_{\mathbf{p}}^2\left(1/\mathrm{H}(\mathbf{p})\right) = -\frac{\left[\mathrm{H}(\mathbf{p})\right]^2\mathrm{H}''(\mathbf{p}) - 2\left[\mathrm{H}'(\mathbf{p})\right]^2\mathrm{H}(\mathbf{p})}{\left[\mathrm{H}(\mathbf{p})\right]^4} \geq 0 \quad \because$$

$$\mathrm{H}(\mathbf{p}) \geq 0 \text{ and } \mathrm{H}''(\mathbf{p}) \leq 0 \tag{29}$$

The second-order derivative is always positive given the nonnegative and concave nature of information entropy. Hence, we can safely conclude that $1/\mathrm{H}(\mathbf{p})$ is a convex function in $\mathbf{p}$.